Electron density fluctuations at interfaces in Nb/Si bilayer, trilayer, and multilayer films: An x-ray reflectivity study

ARTICLE *in* JOURNAL OF APPLIED PHYSICS · MAY 2000

Impact Factor: 2.18 · DOI: 10.1063/1.373479

4 AUTHORS, INCLUDING:

D. M. Phase
UGC-DAE Consortium for Scientific Research
260 PUBLICATIONS **1,513** CITATIONS
SEE PROFILE

Ajay Gupta
Amity University UP, Noida, India
353 PUBLICATIONS **2,452** CITATIONS
SEE PROFILE

Electron density fluctuations at interfaces in Nb/Si bilayer, trilayer, and multilayer films: An x-ray reflectivity study

N. Suresh, D. M. Phase, Ajay Gupta, and S. M. Chaudhari[a)]
Inter University Consortium For DAE Facilities, University Campus, Khandwa Road, Indore-452 017, India

(Received 13 January 2000; accepted for publication 22 February 2000)

A grazing incidence x-ray reflectivity technique has been used to determine electron density profile (EDP) as a function of depth in Nb-on-Si and Si-on-Nb bilayer, Nb–Si–Nb and Si–Nb–Si trilayer, and Nb/Si multilayer structures. In each case, films having layer thicknesses of 35 Å were deposited on float glass and Si(100) substrates under ultrahigh vacuum conditions using an electron beam evaporation technique. EDP determined in as-deposited bilayer films shows that the widths of Si-on-Nb and Nb-on-Si interfaces are 20 and 40 Å, respectively. The large difference observed in the widths is attributed to the different growth morphology of 35 Å Nb and 35 Å Si single layer films as revealed by atomic force microscopy investigations. *In situ* dc resistance measurements carried out on 35 Å single layer Nb films during growth show percolation at a thickness much less than the layer thickness. In case of as-deposited Nb–Si–Nb trilayer film, EDP shows a width of 21 Å at both the interfaces viz. Si-on-Nb and Nb-on-Si whereas in the case of as-deposited Si–Nb–Si trilayer films, the widths of Si-on-Nb and Nb-on-Si interfaces are 21 and 42 Å, respectively. The EDPs obtained from bilayer and trilayer films are used to determine layer-by-layer electron density variation in Nb/Si multilayer structures. The results corresponding to the as-deposited multilayer structure indicate that interdiffusion is larger in the bottom layers of the stack. To study the role of kinetic and thermodynamic factors in the interfacial reactions, the bilayer, trilayer, and multilayer samples were isochronally annealed in vacuum up to a temperature of 300 °C in steps of 50 °C for 1 h. EDP of annealed bilayer and trilayer films show an increase in interfacial width due to interdiffusion of Nb and Si and samples annealed at 250 and 300 °C show Nb-rich and Si-rich intermixed regions. In addition to this, plateau regions having an electron density of 1.8 e/Å^3 are observed in the EDP of Nb–Si–Nb and Si–Nb–Si trilayer structures annealed at 300 °C which indicates the formation of a Nb_3Si phase. Structural parameters obtained from EDP are extended to interpret the results in as-deposited and annealed multilayer structures. The observed contraction in a bilayer period of an annealed multilayer structure is interpreted in terms of formation of a dense Nb_3Si phase confirmed by wide angle x-ray diffraction measurements. Consequently, the multilayer structure is fully destroyed between 250–300 °C. © *2000 American Institute of Physics.* [S0021-8979(00)00611-3]

I. INTRODUCTION

The ability to tune the individual layer thicknesses in nanometer length scale in different types of thin film multilayer structures make them very attractive for various technological applications. From a basic research point of view, these structures provide an ideal platform to study a large number of physical phenomena at different length scales under nonequilibrium conditions. In all these applications, interface quality plays a decisive role in achieving optimum performance for which the multilayer structure is designed.[1–3]

Refractory metal/Si multilayer structures have been extensively studied due to its potential applications in microelectronic devices for making electrical interconnects, as well as in basic research.[4] Metal/Si multilayers provide high reflectivity in the wavelength region 125–250 Å and are used as x-ray mirrors in synchrotron radiation based beamlines.[5] In this respect, both W/Si and Mo/Si multilayer structures have been studied extensively as compared to Nb/Si multilayers, although such multilayer structures are also promising candidates for the above applications.[5,6] Fullerton *et al.*[7] have carried out studies of interfacial roughness in Nb/Si multilayers prepared using a sputtering technique in Ar atmosphere at various pressures. Using cross-sectional transmission electron microscopy (XTEM), wide angle x-ray diffraction (XRD), grazing incidence x-ray reflectivity (XRR) and x-ray diffuse scattering techniques, they have studied the variation in interface roughness and microstructure with the layer thickness, number of layers, and deposition pressure. They further conclude that Si-on-Nb interface is sharper than Nb-on-Si interface and have used XRR modeling to quantify cumulative layer thickness fluctuation, interfacial width parameters, and to identify the existence of an interfacial compound at the Nb-on-Si interface. In a recent report, Wang *et al.*[8] have studied the interdiffusion phenomena in some metal/metal and metal/Si multilayer systems and have determined the diffusion coefficient and activation energy using *in situ* XRR.

In another study conducted on a Nb/Si multilayer system, Zhang *et al.*[9] reported the occurrence of solid-state

a)Author to whom correspondence should be addressed; electronic mail: smc@iucindore.ernet.in

amorphization during deposition at room temperature and initial formation of a Nb_3Si phase in the case of multilayers deposited at 200 °C. These observations have been explained using arguments based on thermodynamic and kinetic considerations. The same group has further extended these investigations to study the effect of deposition conditions on the phase formation and phase selection in Nb/Si multilayers and has observed that the multilayer structures deposited below 500 °C substrate temperature show the existence of crystalline Nb-rich silicide phases.[10] Nakanishi *et al.*[11] have reported the formation of a Nb_3Si phase at an annealing temperature of 550 °C and subsequent formation of silicide multiphases viz. Nb_3Si, Nb_5Si_3, and $NbSi_2$ simultaneously in the sample annealed at 650 °C. Cheng and Chen[12] have investigated the growth kinetics of the amorphous interlayer formed by solid-state diffusion in ultrahigh vacuum deposited polycrystalline Nb on Si(111) substrate. They found that the growth of an amorphous interlayer followed a linear growth law initially in the samples annealed at 450–500 °C and then slows down deviating from linear growth law as a critical thickness of the amorphous interlayer is reached.

In all these reported investigations, refractory metal/Si multilayers were studied mainly using transmission electron microscopy and wide angle XRD. The nature of interfaces viz. Si-on-Nb and Nb-on-Si have been quantified by intensity-contrast scans normal to the layers obtained from the XTEM images. The interpretation based on these images generally suffer from the following drawbacks.[13]

(i) The XTEM images result from projections of the interface over the specimen thickness.
(ii) Intensity-contrast cannot be directly interpreted as the compositional profile of the multilayer structure owing to the nonlinear interaction of the electron beam with the specimen.
(iii) Sample preparation itself may introduce artifacts leading to misinterpretation.
(iv) Microstructural information is obtained only over a highly localized region of the multilayer structure.

In this respect the grazing incidence XRR technique provides powerful characterization of surfaces and interfaces in a nondestructive manner and yields microscopic information (few angstrom) over macroscopic length scales of the order of a few microns which is spatially limited by the coherence area of the x-ray beam.[14] Moreover, recent developments in modeling for the analysis of measured XRR data enables one to extract small changes in electron density which is directly related to the compositional profile of the layer structure.[15,16]

In this article, using the XRR technique and adopting proper modeling and analysis procedures, we have determined the electron density profile (EDP) as a function of depth in Nb-on-Si and Si-on-Nb bilayer films, Nb–Si–Nb and Si–Nb–Si trilayer films, and extended these parameters to derive layer-by-layer electron density variation in Nb/Si multilayer structures. No such systematic study based on bilayers, trilayers, and multilayers has been reported on metal/Si multilayers. Atomic Force microscopy (AFM) and wide angle XRD techniques are employed to correlate the EDP results obtained from XRR with the morphological and structural features. Further, by annealing the samples at intervals of 50 °C in the temperature range 100–300 °C and measuring XRR and wide angle XRD *ex situ* after every stage of annealing, small changes in the EDP taking place due to interdiffusion of Nb and Si have been determined. The results unambiguously show the quantitative variation in the nature of interfaces when Si is deposited on a Nb layer and when Nb is deposited on a Si layer. EDP in the samples annealed at 300 °C clearly shows a region with electron density matching with that of the Nb_3Si phase. These observations are in confirmation with the wide angle XRD results.

II. EXPERIMENTAL DETAILS

Nb/Si bilayer, trilayer, and multilayer samples having layer thickness of 35 Å each were deposited on float glass and Si(100) substrates measuring 15 mm×15 mm using an ultrahigh vacuum e-beam evaporation system. The layer thicknesses were selected on the basis of a layer-by-layer numerical design procedure proposed by Yamamoto and Namioka.[17] The multilayer structure was designed for optimum reflectivity at a wavelength of 135.5 Å at normal incidence. The layer thicknesses determined from the design are 35 Å for each Nb and Si layer which resulted in a normal incidence reflectivity of 50% for 20 layer pairs. For design purpose, the interfaces were considered to be abrupt.

The chamber was evacuated to a pressure of 1×10^{-9} Torr. The deposition of both Nb and Si were carried out at a rate of 0.1 Å/s. During deposition, thickness was measured using a quartz crystal oscillator. The details of the deposition conditions are described elsewhere.[18]

XRR measurements were carried out on a Siemens D5000 diffractometer equipped with a 3 kW sealed Cu tube as the source of the x-rays. The measurements were carried out using a wavelength of 1.542 Å in θ–2θ configuration and the details are described elsewhere.[19] The resolution of the diffractometer in q_z is 0.003 $Å^{-1}$. Wide angle XRD measurements were carried out with the above setup at a fixed grazing incidence angle, just above the critical angle of the film, to limit the penetration of beam to the film thickness.

In situ dc resistance measurements were carried out by a two-probe configuration. Pressure contacts were made on to the silver pads coated independently on the substrate leaving a 1 cm×1 cm area exposed for deposition. The resistance was measured using a Keithley Electrometer (Model 617). The details of the experimental setup are described elsewhere.[20]

AFM measurements were carried out in the contact mode in air using a Digital Instruments Nanoscope III. Different portions of each film were scanned in order to get global information of the sample. The images were acquired on areas varying from 10 μm×10 μm to 0.1 μm×0.1 μm having 256×256 pixels.

Isochronal annealing of the samples was carried out in a resistive heater in a vacuum of 5×10^{-7} Torr. The bilayer, trilayer, and multilayer films were annealed in the temperature range of 100–300 °C in steps of 50 °C for 1 h. The temperature was monitored by a Chromel–Alumel thermocouple and controlled within ±2 °C.

III. XRR MODELING AND DATA ANALYSIS

XRR is an effective nondestructive technique to get the EDP as a function of depth across single and multilayer thin film structures deposited on a substrate. The following procedure was adopted to obtain small variations in EDP from the measured XRR data. The data were analyzed using a model based on the distorted-wave Born approximation[21] (DWBA) and the EDP as a function of depth was determined. Because of the approximations inherent in the model, EDP obtained from DWBA was verified using Parratt's formalism[22] which is based on exact solution of the Helmholtz wave equation. In the samples studied, it was observed that the diffuse scattering[21] intensity is negligible and hence simultaneous analysis of specular and diffuse data is not required.[15] The advantages of this depth graded analysis scheme are;

(i) not only the variation in electron density at the interfaces is considered as is commonly done[23] but also the electron density variation within the layers is determined;
(ii) no specific analytical form of EDP at the interface was assumed.

In the model based on DWBA, the complete film was considered to have a uniform electron density ρ_0 which was taken as the average of the constituent materials weighted with their thicknesses. The complete film was then divided into ''N'' number of thin slices or boxes of equal thickness ''d'' and electron density of the ''i''th box is given as ρ_i $(i=1,...,N)$. The smallest box size, and hence the depth resolution, is inversely proportional to the maximum value of wave vector transfer measured in the experiment.[24] The deviation in electron density of the ith box from the average electron density (AED) ρ_o is defined as $\Delta\rho_i(=\rho_i-\rho_o)$. In this model, the box size must be chosen in a manner so that the interfaces lie between the boxes.[15] The reflectivity of the film as a function of q_Z, calculated using DWBA is given as[24]

$$R(q_Z)=\left| ir_o(q_Z)+\left(\frac{2\pi b}{K}\right)\{a^2(q_Z)\Delta\rho(q_Z^f) + b^2(q_Z)\Delta\rho^*(q_Z^f)\}\right|^2, \tag{1}$$

where $r_o(k)$ is the specular reflectance coefficient of the film with AED ρ_o, $a(q_Z)$ and $b(q_Z)$ are the transmitted and reflected coefficients in this film, $b=e^2/mc^2$ is the classical electron radius, $q_Z(=2\text{ K})=4\pi\sin\theta/\lambda$ and $q_Z^f(=q_Z^2-q_c^2)^{1/2}$ are the normal components of the wave vector transfer in vacuum and film, respectively, and q_c is the critical wave vector transfer in the film. $\Delta\rho(q_Z^f)$ is given as

$$\Delta\rho(q_Z^f)=\left(\frac{i}{q_Z^f}\right)\left\{\sum_{j=2}^{N}(\Delta\rho_j-\Delta\rho_{j-1})\exp(iq_Z^f(j-1)d) + \Delta\rho_1-\Delta\rho_N\exp(iq_Z^fNd)\right\}, \tag{2}$$

where N is the total number of boxes made in the film. The details of the model formulation are described in Ref. 24. The procedure adopted for fitting is as follows: Using prior knowledge about the film from the deposition process, the following structural parameters viz. AED ρ_o, total film thickness, individual box thickness, and hence, the number of boxes are selected. A method based on Fourier transformation of the measured reflectivity data[25] has been used in the present study to select the above parameters prior to actual fitting of the measured data. This was followed by a constrained nonlinear least square fitting of reflectivity numerically calculated using DWBA to the measured reflectivity data, with $\Delta\rho_i(i=1,....N)$ as the fit parameters. The calculated reflectivity was convoluted with a Gaussian instrumental resolution function. For this purpose, a nonlinear least square fitting program based on the Levenberg–Marquardt algorithm[26] has been written in FORTRAN.

To calculate the interfacial width from the EDP, we have adopted the following procedure in all the cases described below consistently. Since the interfacial EDP obtained from the fit does not correspond to any analytical form, the region between a 10% increase in density from the bulk Si value and a 10% decrease from the bulk Nb value is defined as the interfacial width, following the procedure adopted in Ref. 13. This will give a width which is considerably larger than the Debye–Waller factor σ used to quantify the width for a Gaussian density gradient[23] since the Gaussian extends appreciably over $\pm 3\sigma$.

A quick way to get useful information regarding the individual layer thicknesses and the total thickness of the film is to perform Fourier transformation (FT) of the measured reflectivity data. Reflectivity can be written in the Born approximation for wave vectors q larger than q_c as[25]

$$R(q_Z)=\frac{16\pi^2}{q_Z^4}\left|\int_{-\infty}^{+\infty}\rho'(z)\exp(iq_Zz)dz\right|^2, \tag{3}$$

where $\rho'(z)$ is the derivative of the density profile $\rho(z)$ with respect to depth z. The autocorrelation function (ACF) of $\rho'(z)$ is defined as

$$\text{ACF}(z)=\int_{-\infty}^{+\infty}\rho'(u)\rho'(z+u)du, \tag{4}$$

which can be written as[27]

$$\text{ACF}(z)=\int_{-\infty}^{+\infty}R(q_Z)q_Z^4\exp(iq_Zz)dq_Z. \tag{5}$$

Thus, the FT of measured reflectivity directly gives the position of the interfaces. Though the obtained information cannot be easily interpreted in the case of multilayer structures with large number of layers,[27] it provides valuable information in case of simple structures as demonstrated in the present study. The discrete Fourier transformation was performed using a fast Fourier transformation subroutine with a rectangular / Hanning window function.[26] This method has been used effectively in the present study to get information about the individual layer and total film thickness and proves to be helpful in the judicious choice of initial parameters viz. box size and number of boxes for the least square fitting

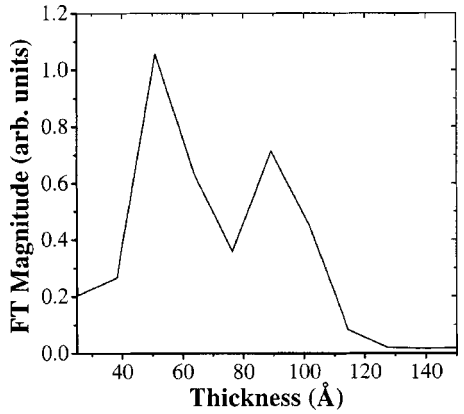

FIG. 1. Fourier transformation of measured XRR data of Si-on-Nb bilayer deposited on float glass substrate.

operations. Moreover, since this process does not involve least square fitting, unambiguous information is obtained. This procedure was adopted for all the samples in the present study. We present here only one such curve. ACF determined from the measured reflectivity data of Si-on-Nb bilayer deposited on float glass substrate plotted in Fig. 1 shows peaks at 50 and 90 Å corresponding to the position of Si/Nb and Nb/substrate interfaces, respectively. The measured XRR data, of which ACF is shown in Fig. 1, corresponds to the one shown in Fig. 3(a).

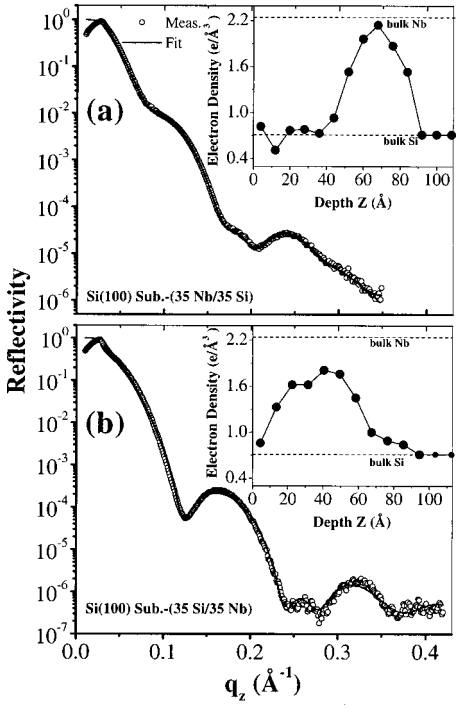

FIG. 2. XRR scans (open circles) and calculated reflectivities (line) of as-deposited (a) Si-on-Nb bilayer and (b) Nb-on-Si bilayer samples on Si(100) substrate. The inset shows their corresponding EDPs (closed circles). The line connecting the closed circles is a guide to the eye.

IV. RESULTS AND DISCUSSION

A. Bilayer films (as-deposited)

To examine the nature of interfaces in the case of Si-on-Nb and Nb-on-Si, the bilayer samples were deposited on Si(100) substrates under identical conditions. Figures 2(a) and 2(b) show the measured XRR data along with the fitted spectra of Si-on-Nb and Nb-on-Si bilayers, respectively, as a function of the wave vector transfer q_Z. The lowering of the measured reflected intensity for very small wave vector transfers is due to the fact that at extreme grazing angles, the footprint of the beam is larger than the sample size. The *inset* shows their corresponding EDPs obtained from the fit to the measured XRR data. For the sample shown in Fig. 2(a), 11 boxes each of 8.0 Å size were made and for the sample shown in Fig. 2(b), 10 boxes each of 9.0 Å size were considered. The average electron density ρ_o was taken as 1.25 and 1.36 e/Å^3 for Si-on-Nb and Nb-on-Si samples, respectively. The linear absorption coefficient μ for the films were taken as 6×10^{-6} and 5×10^{-6} Å^{-1} for the above samples, respectively. The last three boxes are added in the EDP to indicate the position and electron density of the substrate. This convention has been adopted in all the EDP figures. The total film thickness in both the samples was found to be 90 Å from the fit to the measured XRR data. It is clearly seen from the respective EDPs [*Inset* of Figs. 2(a) and 2(b)] that there is a striking difference in the nature of the two interfaces viz. Si-on-Nb and Nb-on-Si. In the case of the Si-on-Nb bilayer [Fig. 2(a)], the deposited Nb layer shows a density close to its bulk value (2.24 e/Å^3) at the middle of the layer thickness. Further, gradation in electron density at the interface between Si and Nb is also seen and the interfacial width calculated from the EDP using the criteria described earlier is 21 Å. The EDP corresponding to the Nb-on-Si bilayer [Fig. 2(b)] exhibits interesting features. The electron density of the Si layer deposited on the substrate obtained in this case ($\sim$1.0 e/Å^3) is considerably higher than its bulk value (0.71 e/Å^3). In addition to this, a gradation in the electron density, increasing towards the Nb side of the interface is observed showing a drastic difference in the nature of the EDPs in the two bilayers. The observed difference can be explained if one considers that in the case of the Nb-on-Si bilayer, the Si layer of 35 Å thickness deposited on Si(100) substrate may not have formed a continuous film but a sort of porous structure would have formed. During subsequent deposition of the Nb layer on such a porous Si film, Nb atoms would get incorporated in the open spaces between the small Si clusters. This will result in a larger electron density of the Si layer compared to its bulk value. The corresponding electron density of the Nb layer is 80% of its bulk value. This lower value of the electron density is due to the oxidation of the Nb layer, since Nb has high affinity for oxygen and acts as an efficient getter material for oxygen. Since the Nb layer is fully oxidized, the interfacial width of Nb-on-Si is not calculated in this case. In order to isolate the effect of oxidation and to study the true nature of the interfaces, the above samples were prepared with a 25 Å thick protective capping layer of carbon. The error bars to the electron densities determined after convergence of the fit is typically $\sim$0.03 e/Å^3 and are not indicated in the figures for clarity.

Figures 3(a) and 3(b) show the measured and fitted XRR spectra of Si-on-Nb and Nb-on-Si bilayers with a 25 Å thick

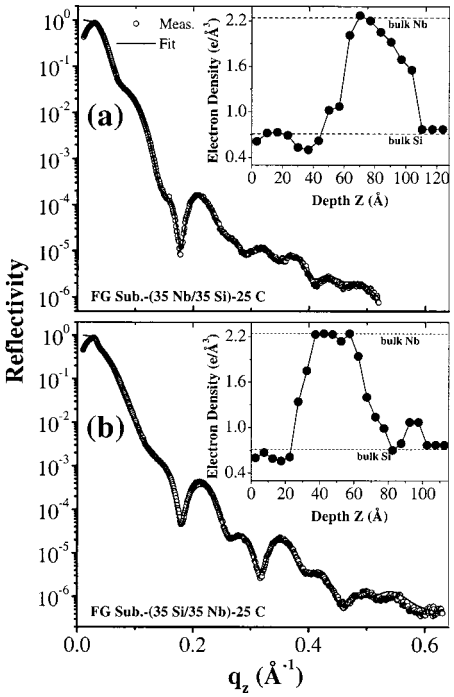

FIG. 3. XRR scans (open circles) and calculated reflectivities (line) of as-deposited (a) Si-on-Nb bilayer and (b) Nb-on-Si bilayer samples capped with a 25 Å carbon layer on float glass substrate. The inset shows their corresponding EDPs (closed circles). The line connecting the closed circles is a guide to the eye.

carbon cap layer deposited on float glass substrate. The *inset* shows their corresponding EDPs. To obtain the EDP from the XRR data, we have considered 16 boxes each of 6.7 Å size for the Si-on-Nb bilayer [Fig. 3(a)] and 20 boxes each of 5.0 Å size for the Nb-on-Si bilayer [Fig. 3(b)]. The fitting was carried out using an average density ρ_o of 1.47 e/Å^3 and linear absorption coefficient μ of 6.7×10^{-6} Å^{-1} for both the samples. EDP of carbon capped Si-on-Nb bilayer shown as an *inset* in Fig. 3(a) indicates that the deposited Nb layer density corresponds to its bulk value. However, the Si layer deposited on the Nb layer shows a density which is 80% of bulk Si. For deposited Si, density up to 20% lower than bulk has been reported due to its amorphous nature.[28] Carbon layer extends over a width of four boxes (depth $Z=0-27$ Å) and has an electron density close to that of Si. The electron density of float glass (FG) was determined to be 0.77 e/Å^3 from XRR measurements on FG substrate. An EDP of carbon capped Nb-on-Si bilayer, shown as an *inset* in Fig. 3(b), shows similarity to the observations made in Fig. 2(b) in the case of a Si layer. In this case also, the Si layer shows a density much higher than its bulk value. As explained earlier, this is because the Nb atoms get embedded during deposition onto the porous structure of Si film deposited on the float glass substrate. This feature is observed in the films deposited on Si(100) [Fig. 2(b)] as well as on float glass substrate [Fig. 3(b)]. Moreover, the effect of the carbon capping layer is clearly seen in this case as the top Nb layer shows a bulk density in contrast to Fig. 2(b). Thus, the carbon layer protects the underlying film bringing out the true nature of the growth of the layers. The widths of Si-on-Nb and Nb-on-Si interfaces are 20 and 40 Å, respectively. The interface between C and Nb is relatively sharp and has a width of two boxes, i.e., 10 Å. The larger width of the Nb-on-Si interface compared to the Si-on-Nb interface is due to the incorporation of Nb atoms into the entire Si layer. This asymmetry in the interfacial profile has been observed for a number of metal/Si multilayer systems with the metal-on-Si interface width consistently being larger than the Si-on-metal interface.[7] This difference has been generally attributed to the following factors.

(i) Higher kinetic energy of the metal adatoms impinging on the Si layer as is the case in sputter deposition of thin films.[29] However, asymmetric interfacial profile is observed in the present study in films prepared by evaporation where kinetic energy of the adatoms are of the order of 0.2 eV. This suggests that kinetic energy of the adatoms may not play a major role in the formation of asymmetric interfaces.

(ii) The release of the latent heat of condensation may induce some interdiffusion and has been reported in the literature.[30]

(iii) Enhanced Si diffusion into the forming metal layer relative to diffusion into the already deposited metal layer.[29]

In thin film multilayer structures, layer thicknesses involved are in the nanometer length scale and hence morphology of the individual deposited layer may also play a vital role in deciding the nature of interfaces. In order to test the validity of this aspect as an additional factor responsible for the observed asymmetric interfacial profile, we have carried out the morphological study of such layers. For this investigation, AFM images of 35 Å single layer films of Nb and Si deposited on both Si(100) and float glass substrates under identical conditions as those used for preparation of bilayers were recorded. More than ten different portions of each sample were scanned over areas varying from $10\,\mu$m $\times10\,\mu$m to $0.1\,\mu$m$\times0.1\,\mu$m to get a global picture of the growth. Figure 4(a) shows a $5\,\mu$m$\times5\,\mu$m AFM picture of 35 Å Si layer deposited on float glass substrate. It can be clearly seen that 35 Å Si forms a highly porous structure on the substrate. When an Nb layer is deposited on the Si layer, Nb atoms will get embedded during deposition in the vacant portions. This will result in the Si layer having a density considerably higher than bulk Si. This, indeed, is reflected in the measured XRR spectra shown in Figs. 2(b) and 3(b). Figure 4(b) shows a $5\,\mu$m$\times5\,\mu$m AFM picture of 35 Å Nb layer deposited on float glass substrate. In this case, it can be clearly observed that 35 Å Nb layer exhibits a much higher coverage than the 35 Å Si layer. Moreover, the growth morphology of Si and Nb layers were found to be similar on a Si(100) substrate, and hence are not shown here. The images shown in Figs. 4(a) and 4(b) are selected out of several images scanned over different portions of the films so as to represent the global morphology. The observed growth behavior provides a real space evidence to conclude that the growth morphology of individual layers play an important role in contributing to the observed difference between Si-on-Nb and Nb-on-Si interfacial widths.

To further support the above results, we monitored the dc resistance of Nb film during growth in a separate experiment under identical conditions by a two-probe configuration and the resistance as a function of thickness is plotted in Fig.

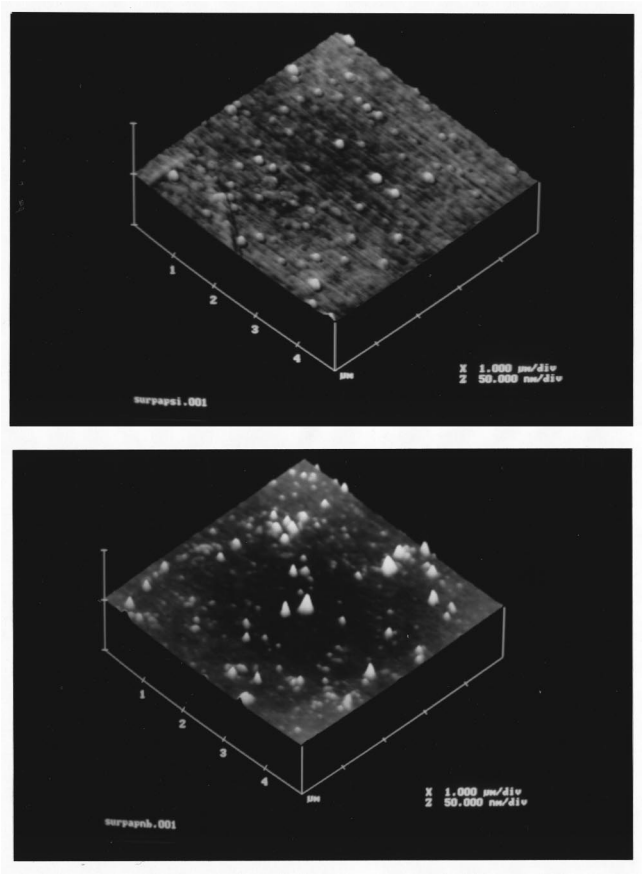

FIG. 4. Atomic force micrographs of (a) 35 Å Si layer and (b) 35 Å Nb layer deposited on float glass substrate.

5. It can be observed in Fig. 5 that there is an initial sudden drop in resistance to ~10 MΩ/□ at a thickness of 4Å with a further steep decrease in resistance to ~10 kΩ/□ at a thickness of 10 Å. This is followed by a slow decrease in resistance to a value of ~1 kΩ/□ at a thickness of 25 Å. The corresponding thicknesses involved are much less than the Nb layer thickness (35 Å) involved in the present study suggesting that 35 Å Nb forms a closed layer. Similar types of measurements have been reported recently to show the continuity of deposited Mo and Co layers in Mo/Al_2O_3 and Co/Al_2O_3 multilayers respectively.[31,32]

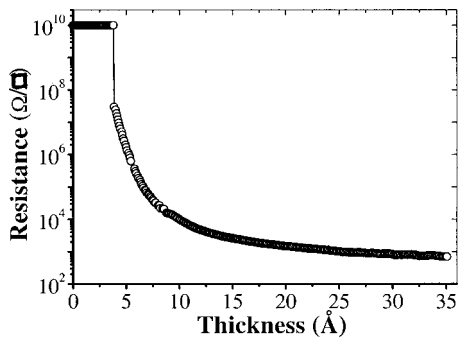

FIG. 5. Direct current electrical resistance measured *in situ* during deposition of 35 Å thick Nb layer on float glass substrate. The solid line connecting the circles is a guide to the eye.

B. Bilayer films (annealing studies)

Thermal annealing of the samples were carried out to study the diffusion and solid state reactions taking place at the interface between Nb and Si. From the reported literature on metal/Si systems, it is observed that interfacial reactions can be considered as the interplay of thermodynamic and kinetic factors. The study of interfacial reactions in the present system is motivated due to the following reactions: (i) The Nb/Si system exhibits negative free energy of mixing over a wide range of compositions.[9] This provides the large thermodynamic driving force for the formation of amorphous or crystalline niobium silicide phases at the interface. This approach can predict the trend in the interfacial reactions using the immediate minimization of free energy. However, the phase selection in the interfacial reactions is controlled by kinetic constraints because the difference between the driving forces for the formation of amorphous and crystalline niobium silicides is not substantially large.[9] The first nucleated phase in the interfacial reaction between metal and Si is of considerable interest for their applications. Though several equilibrium metal silicide phases exist in the phase diagram, it has been generally shown that only one phase grows at a time. This has been explained by the fact that growth of the silicide is a kinetic phenomenon.[11] (ii) Another important aspect of this study has been the determination of the dominant diffusing species in metal/Si interfacial reactions. Though Si is reported to be the dominant diffusing species due to its smaller atomic size, 1.46 and 1.32 Å for Nb and Si respectively, it has not been determined unambiguously.[10]

In the present study, the samples were annealed in the temperature range 100–300 °C in steps of 50 °C for 1 h. The same sample was successively annealed at higher temperatures. XRR and XRD measurements were carried out *ex situ* after every stage of annealing. By determining the small fluctuations in the electron density and correlating them with the structural parameters derived from wide angle XRD, the results are discussed in light of the kinetic and thermodynamic aspects. For the annealing study, two types of bilayer samples viz. Si-on-Nb bilayer without a carbon cap layer and Nb-on-Si bilayer with a carbon cap layer are selected for the following reasons. As observed in the EDPs of the as-deposited bilayers, Nb layers, when exposed to the ambient, get completely oxidized and hence a Nb-on-Si bilayer capped with a 25 Å thick carbon layer was chosen. A Si-on-Nb bilayer without a carbon capping layer was chosen for the following reasons: (i) The Si layer, when exposed to the ambient, forms a thin SiO_2 layer (~ 15 Å) which is stable thereby preventing further oxidation.[28] This is clearly observed in the results to be described below where the underlying Nb layer is protected and shows density corresponding to its bulk value. (ii) Since the electron density contrast between carbon and Si is very less, reflectivity is less sensitive to the C/Si interface. We noticed that this causes difficulty in getting a good fit to the data.

Figures 6(a)–6(e) show the measured and fitted XRR spectra of as-deposited Si-on-Nb bilayer sample on float glass substrate along with samples annealed at 100, 200, 250, and 300 °C, respectively. For fitting the data, 12 boxes each

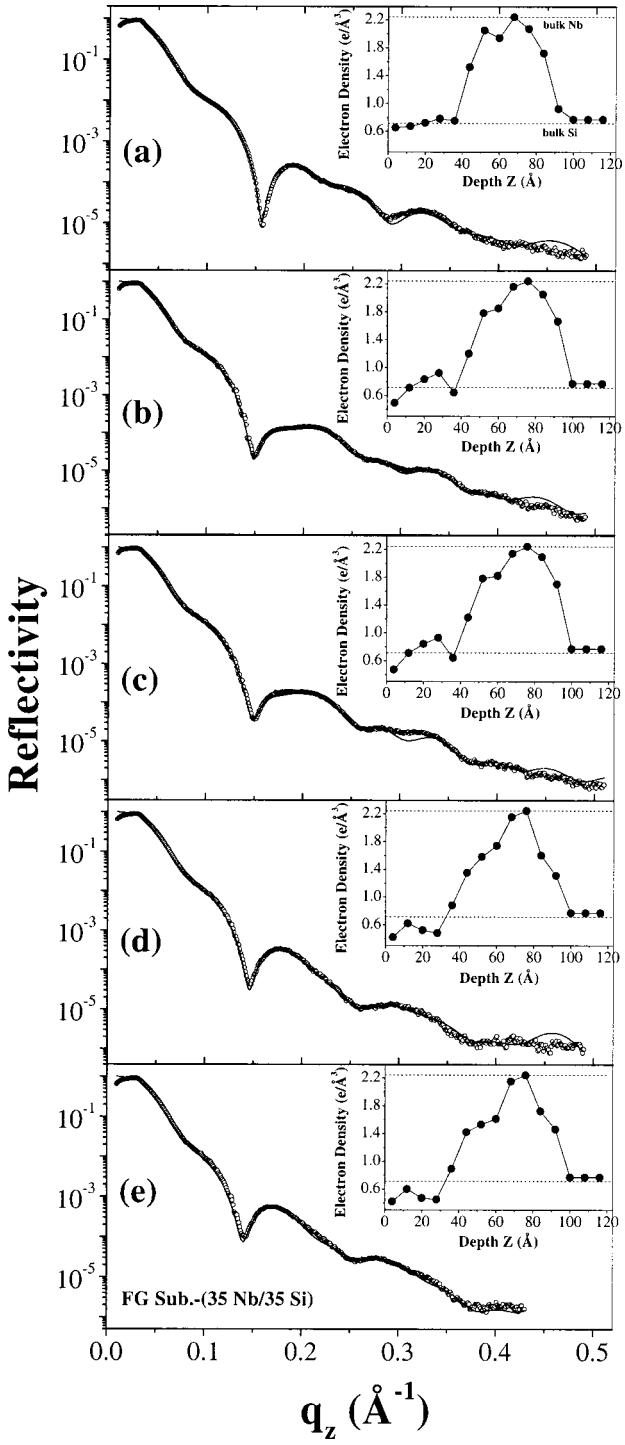

FIG. 6. XRR scans (open circles) and calculated reflectivities (line) of (a) as-deposited Si-on-Nb bilayer sample on float glass substrate and annealed at (b) 100 °C, (c) 200 °C, (d) 250 °C, and (e) 300 °C. Inset shows their corresponding EDPs (closed circles) derived from the fit. The line connecting the circles is a guide to the eye.

of 8.0 Å size were considered. The average density ρ_0 and linear absorption coefficient μ for the film were taken as 1.42 e/Å^3 and 6×10^{-6} Å^{-1}, respectively. Their corresponding EDPs derived from the fit are shown in the inset. The amplitude of oscillations in the reflectivity spectrum is proportional to the electron density contrast at the interfaces. The measured spectra show the variation in amplitude of the interference oscillations with annealing temperature. By carrying out fitting of the measured data using the box model, information about the nature of the interfaces in each case have been extracted from the determined EDP. EDP of as-deposited Si-on-Nb bilayer [inset of Fig. 6(a)] shows the Nb layer having bulk density at the center of the layer. This shows that the thin SiO_2 layer formed at the top protects the Nb layer from the ambient. The width of the Si-on-Nb interface calculated from the EDP is 24 Å (three boxes) indicating that there is considerable mixing of Nb and Si even in the as-deposited state. After annealing at 100 °C, a change in the EDP at the Si-on-Nb interface [inset of Fig. 6(b)] is observed and the interfacial width increases to 40 Å (five boxes) due to the interdiffusion of Nb and Si. After annealing at 200 °C [inset of Fig. 6(c)], there is no significant modification of the interface. XRR spectrum of the sample annealed at 250 °C [Fig. 6(d)] shows drastic changes in the interference oscillations. The corresponding EDP [inset of Fig. 6(d)] shows that considerable changes have taken place in the electron density at the interface. EDP of the sample annealed at 300 °C [inset of Fig. 6(e)] clearly shows three distinct regions: An Si-rich region, an Nb-rich region, and a plateau region at the interface with an electron density of ~1.5 e/Å^3. The plateau extends over a width of three boxes, i.e., 24 Å between $Z = 40-65$ Å [inset of Fig. 6(e)]. It has been verified in all the annealed samples that the electron density summed over all the boxes is conserved. The width of the Si-on-Nb interface at different temperatures of annealing calculated from the EDPs [inset of Figs. 6(a)–6(e)] are summarized in Table I. It can be observed from the inset of Figs. 6(a)–6(e) and Table I that though there is no change in the interfacial width (calculated using the criteria described earlier) within the precision of the box size in the temperature range 100–300 °C, considerable changes in the electron density at the interface region has taken place. Such a behavior has been reported in the Nb/Si system where it was observed that diffusion is inhibited after a critical thickness of the amorphous interlayer is reached.[12] The amorphous Nb silicide interlayer formed acts as an interdiffusion barrier to impede further growth of the amorphous Nb silicide layer. Since the difference between the energies for the formation of amorphous or crystalline silicide is small,[9] it is possible that further annealing causes crystallization of the amorphous Nb silicide interlayers.

TABLE I. Widths of Si-on-Nb and Nb-on-Si interfaces calculated from the EDP of corresponding bilayer films (Figs. 6 and 7, respectively) at different annealing temperatures.

Annealing temperature (°C)	Si-on-Nb interface width (Fig. 6) (Å)	Nb-on-Si interface width (Fig. 7) (Å)
As-deposited	24	40
100	40	40
200	40	50
250	40	55
300	40	55

From the EDPs, it can be clearly seen that the interfacial profile cannot be fit to any particular analytical form. Gener-

ally, the loss in specular reflectivity due to finite interfacial width is accounted for by using equations for analytical interface profiles (error function, exponential, and linear) which are derived in Ref. 33. This may not yield the true picture of processes taking place in the sample in all the cases. Hence, it becomes imperative to fit the data with a graded density profile.

Figures 7(a)–7(e) show the measured and fitted XRR spectra of an as-deposited Nb-on-Si bilayer sample capped with a 25 Å thick carbon layer on float glass substrate along with samples annealed at 100, 200, 250, and 300 °C, respectively. For fitting the data, 20 boxes each of 5.0 Å size were considered. The average density ρ_0 and linear absorption coefficient μ for the film were taken as 1.47 e/Å^3 and 6.7 $\times 10^{-6}$ Å^{-1} respectively. Their corresponding EDPs derived from the fit are shown in the inset. The as-deposited sample is identical to that shown in Fig. 3(b) and its XRR spectrum and EDP are shown in Fig. 7(a) for comparison. The width of the Nb-on-Si interface calculated from the EDP is 40 Å. XRR data of the sample annealed at 100 °C [Fig. 7(b)] shows no change in the EDP. After annealing at 200 °C, a marginal reduction in the amplitude of oscillations in the measured reflectivity is observed at higher q_z values [Fig. 7(c)]. From the corresponding EDP [inset of Fig. 7(c)], it is observed that there is a decrease in the electron density of the Nb layer at the Nb/Si interface. This is attributed to the diffusion of Si atoms into the Nb layer. The width of the Nb-on-Si interface increases to 50 Å. This effect is more pronounced at 250 °C [inset of Fig. 7(d)] where a further decrease in the electron density of the Nb layer at the Nb/Si interface is observed. A vital information regarding the dominant diffusing species in metal/Si interfacial reactions can be derived from the above EDPs [inset of Figs. 7(c) and 7(d)]. As explained earlier, there is considerable debate in this area with no clear experimental evidence available.[10] From the inset of Figs. 7(c) and 7(d) which show a decrease in the electron density of the Nb layer at the interface, it can be clearly said that Si atoms are more mobile in this temperature range. This is useful information in understanding the metal–silicon diffusion phenomena. Another feature that can be noted is that the interface between C and Nb remains unaffected up to 250 °C. The XRR spectrum of the sample annealed at 300 °C shows significant changes [Fig. 7(e)]. The relative amplitudes of the interference oscillations are completely changed suggesting that considerable modifications have taken place in the layer structure. Corresponding EDP [inset of Fig. 7(e)] reveals that the layer structure is fully destroyed and the interface profile is nearly linear. Further, it can also be observed that the C/Nb interface shows changes compared to earlier cases suggesting reaction between Nb and C at 300 °C. In addition to this, it can be seen from the inset of Figs. 7(a)–7(e) that the nature of EDP in the Si layer over a depth of 85–105 Å, where Nb atoms are incorporated during deposition, remains unchanged from the as-deposited sample to the sample annealed up to 300 °C. The width of the Nb-on-Si interface at different temperatures of annealing calculated from the EDPs [inset of Figs. 7(a)–7(e)] are compared with those of Si-on-Nb bilayer in Table I.

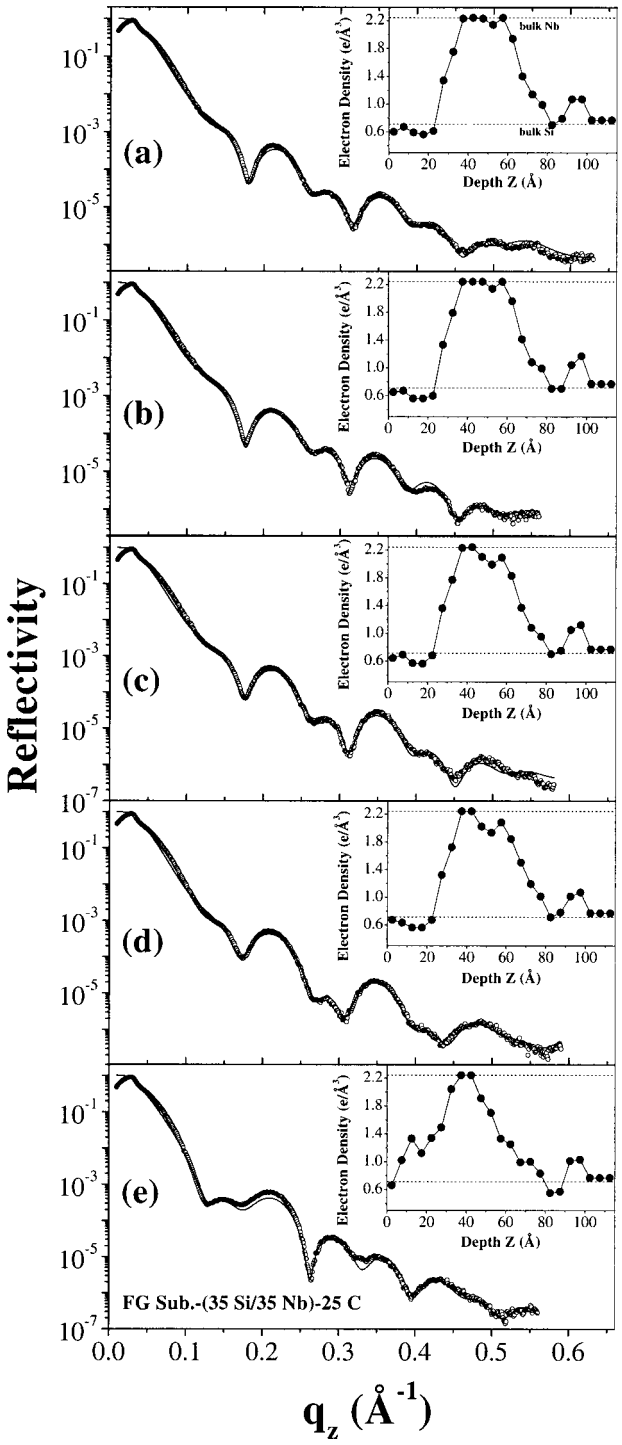

FIG. 7. XRR scans (open circles) and calculated reflectivities (line) of (a) as-deposited Nb-on-Si bilayer sample capped with a 25 Å carbon layer on float glass substrate and annealed at (b) 100 °C, (c) 200 °C, (d) 250 °C, and (e) 300 °C. Inset shows their corresponding EDPs (closed circles) derived from the fit. The line connecting the circles is a guide to the eye.

C. Trilayer films (as-deposited and annealed)

As a next step towards understanding the growth of the multilayer structure in the Nb/Si system, two types of trilayer films viz. Nb–Si–Nb and Si–Nb–Si were deposited on float glass substrate under identical conditions to study the effect of annealing. The Nb–Si–Nb trilayer film with layer thick-

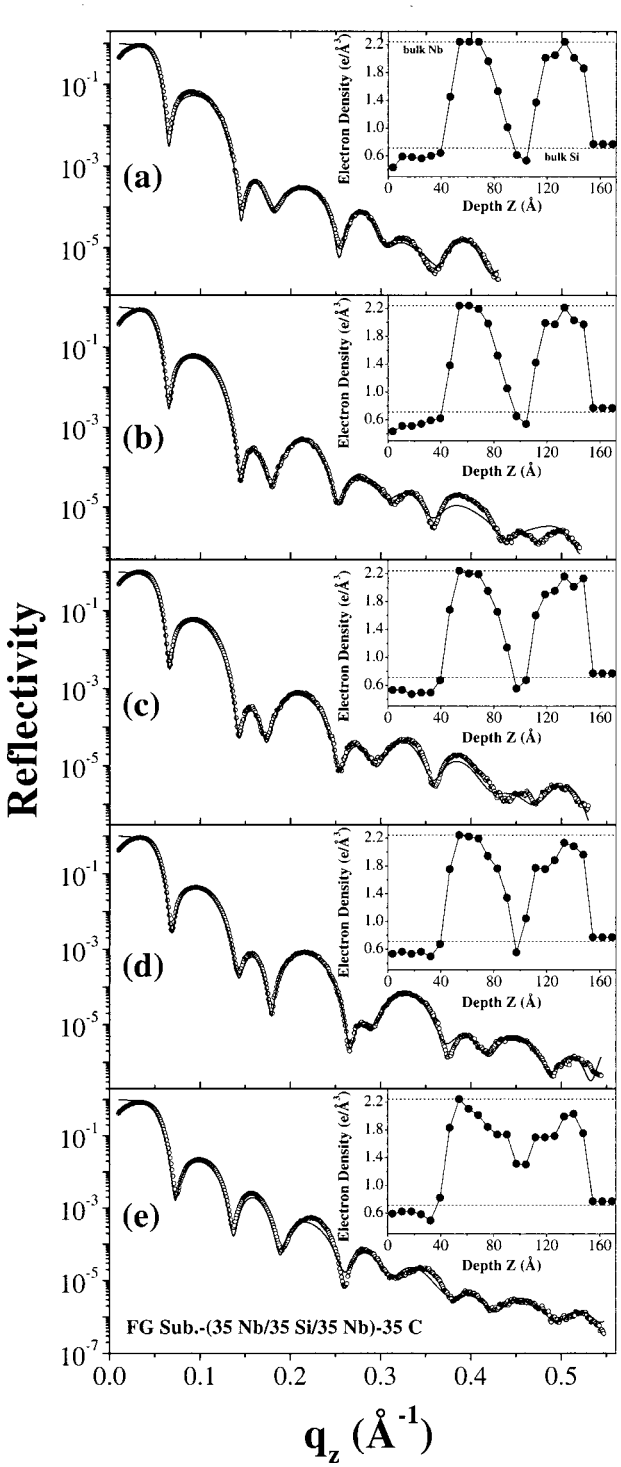

FIG. 8. XRR scans (open circles) and calculated reflectivities (line) of (a) as-deposited Nb–Si–Nb trilayer sample capped with a 35 Å carbon layer on float glass substrate and annealed at (b) 100 °C, (c) 200 °C, (d) 250 °C, and (e) 300 °C. Inset shows their corresponding EDPs (closed circles) derived from the fit. The line connecting the circles is a guide to the eye.

ness of 35 Å each was capped with a 35 Å carbon layer. In this sample, the Si layer is sandwiched between two Nb layers. Figures 8(a)–8(e) show the measured and fitted XRR spectra of an as-deposited Nb–Si–Nb trilayer sample capped with a 35 Å thick carbon layer on float glass substrate along with samples annealed at 100, 200, 250, and 300 °C, respectively. For fitting the measured data, 21 boxes each of 7.2 Å size were considered. The average density ρ_0 and linear absorption coefficient μ for the film were taken as 1.73 e/Å^3 and 6×10^{-6} Å^{-1}, respectively. The higher value of ρ_0 considered for the calculations compared to the bilayer films is essentially due to the higher concentration of Nb in the trilayer structure. Their corresponding EDPs derived from the fit are shown in the inset. The EDP of the as-deposited sample [inset of Fig. 8(a)] shows that both the Nb layers have electron densities matching their bulk value. The Si layer has a electron density lower than its bulk value and is attributed to reasons explained earlier [Fig. 3(a)]. In this case also, the effect of the protective carbon capping layer similar to the bilayer sample is observed. The interface between C and Nb is relatively sharp and has a width of one box, i.e., 7.2 Å. The widths of the two interfaces viz. Si-on-Nb and Nb-on-Si determined from EDP are identical and is equal to 21 Å. On the contrary, the interfacial widths obtained from the corresponding bilayer samples were 24 and 40 Å, respectively (see Table-I). When one compares these interfacial widths with the corresponding bilayer samples, a major difference is observed only in the width of the Nb-on-Si interface. This observation can be explained on the basis of the different growth morphology of a Si layer when deposited on a 35 Å thick Nb layer. This is evident from the EDP shown in the inset of Fig. 8(a) where two boxes in the middle of the Si layer ($Z=94-108$ Å) show the density of amorphous Si. This clearly shows that Nb atoms are not incorporated into the entire Si layer deposited on the Nb layer. The EDP of the sample annealed at 100 and 200 °C [inset of Figs. 8(b) and 8(c)] shows a marginal decrease in the electron density of the top and bottom Nb layers at the interface with Si. This is in confirmation with the observations made from the inset of Figs. 7(c) and 7(d) in the bilayer film. This again suggests that Si is the dominant diffusing species in this temperature range. The EDP of the sample annealed at 250 °C [inset of Fig. 8(d)] shows considerable changes in the electron density at Nb-on-Si and Si-on-Nb interfaces. It is also observed that the interface between C and Nb is unaffected after annealing at 250 °C. XRR data of the sample annealed at 300 °C [Fig. 8(e)] shows drastic reduction in the amplitude of the interference oscillations. This suggests that considerable reduction in the electron density contrast at the interfaces has taken place. Corresponding EDP derived from the fit [inset of Fig. 8(e)] shows that the layer structure is fully destroyed with no clear demarcation between the two interfaces. The EDP shows the following interesting features. A plateau region having an electron density of $\sim$ 1.8 e/Å^3 extending over a width of three boxes, i.e., 21 Å at the Si-on-Nb interface and two boxes, i.e., 14 Å at the Nb-on-Si interface can be clearly seen. Another region having an electron density of 1.3 e/Å^3 and extending over a width of two boxes, i.e., 14 Å can also be clearly seen. This suggests that there are Nb-rich and Si-rich intermixed regions. The widths of the Si-on-Nb and Nb-on-Si interfaces at different temperatures of annealing calculated from the EDPs [inset of Figs. 8(a)–8(e)] are summarized in Table II. Out of the different stable phases of niobium silicide in the phase diagram,[9] electron density of 1.8 e/Å^3 matches with that of the Nb_3Si phase.[34] It can be observed from Table II that though there is no significant

TABLE II. Widths of Si-on-Nb and Nb-on-Si interfaces calculated from the EDP of carbon capped Nb–Si–Nb trilayer film (Fig. 8) at different annealing temperatures.

Annealing temperature (°C)	Si-on-Nb interface width (Fig. 8) (Å)	Nb-on-Si interface width (Fig. 8) (Å)
As-deposited	21	21
100	21	21
200	21	21
250	28	21
300	-	-

change in the interfacial widths calculated using the criteria described earlier up to a temperature of 250 °C, there are considerable modifications in the electron density at both the interfaces [inset of Figs. 8(a)–8(e)]. After annealing at 300 °C, the width of the C/Nb interface increases to two boxes, i.e., 14.4 Å.

In the Si–Nb–Si trilayer structure, the thickness of top Si layer was increased to 50 Å (35 Å + 15 Å protective layer) while the underlying Nb and Si layers had a thickness of 35 Å each. In this case, the Nb layer is sandwiched between two Si layers. Figures 9(a) and 9(b) show the measured and fitted XRR spectra of as-deposited and 300 °C annealed Si–Nb–Si trilayer samples, respectively. The sample was subjected to the same annealing procedure as described for the earlier trilayer sample. The results of only the as-deposited and 300 °C annealed samples are discussed here. For fitting the data, 19 boxes each of 6.95 Å size were considered. The average density ρ_0 and linear absorption coefficient μ for the

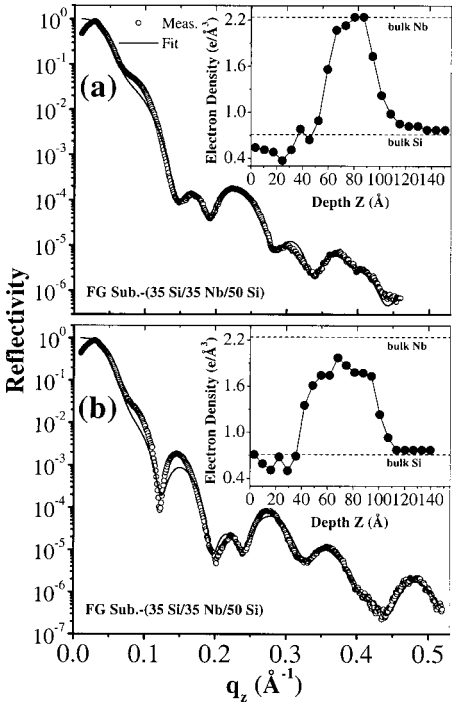

FIG. 9. XRR scans (open circles) and calculated reflectivities (line) of (a) as-deposited Si–Nb–Si trilayer and (b) Si–Nb–Si trilayer sample annealed at 300 °C. The inset shows their corresponding EDPs (closed circles). The line connecting the closed circles is a guide to the eye.

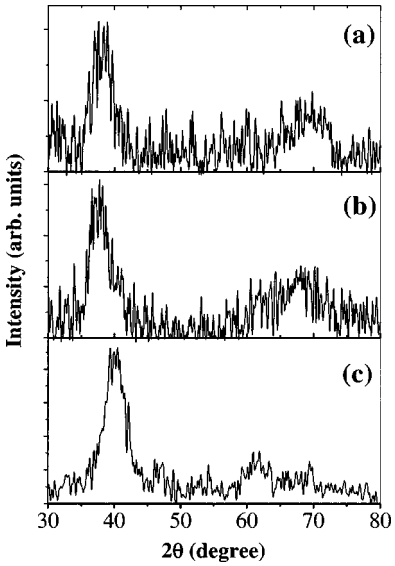

FIG. 10. Wide angle XRD patterns of (a) as-deposited $(35\,\text{Nb}/35\,\text{Si})_{10}$ multilayer sample on float glass substrate and annealed at (b) 300 °C and (c) 400 °C.

film were taken as 1.02 e/Å^3 and 5×10^{-6} Å^{-1}, respectively. The inset shows their corresponding EDPs derived from the fit. In the as-deposited sample, the Si layer deposited on the substrate shows a density higher than its bulk value, due to the reasons explained earlier. The widths of Si-on-Nb and Nb-on-Si interfaces calculated from the EDP are 21 and 42 Å, respectively. The widths are in confirmation with the values obtained in the corresponding bilayer films and the small difference is due to the different box sizes (see Table-I). The EDP of the sample annealed at 300 °C [Inset of Fig. 9(b)] shows that the layer structure is fully destroyed with no clear demarcation between the two interfaces. In this case again, a plateau region having an electron density of $\sim$ 1.8 e/Å^3 can be clearly observed at the Si-on-Nb and Nb-on-Si interfaces, indicating the formation of a Nb_3Si phase.

D. Multilayer structure (as-deposited and annealed)

To support the conclusions drawn from the EDP results of trilayer samples, wide angle x-ray diffraction measurements were carried out on a multilayer structure of the same layer thicknesses (35 Å each) with ten bilayers $[(35\,\text{Nb}/35\,\text{Si})_{10}]$ to have significant volume fraction for detectable diffraction signal. XRD spectrum of as-deposited multilayer [Fig. 10(a)] shows peaks at $2\theta = 38.4°$ and 69.7° corresponding to (110) and (211) reflections of Nb suggesting that the Nb layers are polycrystalline in nature. The peak positions were determined by fitting a pseudo-Voigt function independently to each reflection. The grain size normal to the surface determined from Nb(110) reflection using the Scherrer formula[35] was ~27 Å which indicates that the structural coherence length is less than the Nb layer thickness. XRD spectrum of the multilayer annealed at 300 °C [Fig. 10(b)] shows peaks at $2\theta = 37.6°$ and 68.4° which correspond to the Nb_3Si phase[34] and is in total agreement with the results obtained from EDP [inset of Figs. 8(e) and 9(b)]. To the best of our knowledge, this is the first report in which EDP derived

from XRR precisely shows the density of the interfacial compound phase observed in wide angle XRD data. It has been reported on the basis of thermodynamic free energy considerations that Nb_5Si_3 should be the first phase formed during interfacial reactions since it has the largest driving force.[9] But experimentally, it has been well established for several metal/Si systems that the first phase formed is not the one with the lowest heat of formation (ΔH).[36,37] In this context, it is essential that the available concentration of the reacting elements at the interface and the concentration of the reactants in the silicide phase are also considered. This is mainly influenced by the mobilities of the reacting species and hence the kinetic factors play a major role in deciding the first phase formed. Thus, the true driving force for the interfacial reactions depends on the modified heat of formation (ΔH^*) and is given as[37]

$$\Delta H^* = \Delta H \frac{\text{available concentration of Si atoms}}{\text{concentration of Si atoms in the silicide phase}}, \tag{6}$$

thereby linking thermodynamics and kinetics. This model correctly predicts that Nb_3Si should be the first nucleating phase as it has the lowest modified heat of formation.[9] Based on thermal annealing studies carried out on 1300 Å Nb sputter deposited on single crystal Si(100) substrate, Nakanishi *et al.*[11] have reported that Nb_3Si is the first phase to nucleate in Nb/Si interfacial reactions after annealing at 550 °C. Further, they have observed that Nb_3Si and Nb_5Si_3 coexist after annealing at 600 °C and finally $NbSi_2$ was found to be the only existing phase after annealing at 700 °C. To determine the nucleating phase at higher temperatures in the present study, we annealed the multilayer structure at 400 °C and the corresponding XRD spectrum is shown in Fig. 10(c). The peaks are observed at $2\theta = 40.2°$ and 61.4° which correspond to the $NbSi_2$ phase.[34] The basic differences between the observations reported in Ref. 11 and our results are in the magnitude of the temperatures at which the corresponding phases are formed and in the much larger layer thickness involved in the study reported in Ref. 11. Moreover, coexistence of multiple Nb-rich silicide phases were not observed in the present study. This could be due to considerable scatter present in the wide angle XRD data because of the small volume fraction available for diffraction.

With the knowledge about the nature of Nb-on-Si and Si-on-Nb interfaces which appear alternately in a multilayer structure, we have deposited Nb/Si multilayer with five and ten bilayers under identical conditions on float glass and Si(100) substrates. Only the results of as-deposited and annealed Nb/Si multilayer with five bilayers are shown in Figs. 11(a)–11(c). The inset shows the corresponding ACF of the density gradient obtained by Fourier transformation of the measured reflectivity data.[27] Figure 11(a) shows the measured and fitted XRR spectra of as-deposited Nb/Si multilayer with five bilayers [$(35\,\text{Nb}/35\,\text{Si})_5$] deposited on float glass substrate. The measured critical wave vector transfer q_c corresponds to an electron density of 1.5 e/Å^3 and is equal to the average electron density of the multilayer structure. The spectrum shows Bragg peaks upto the fifth

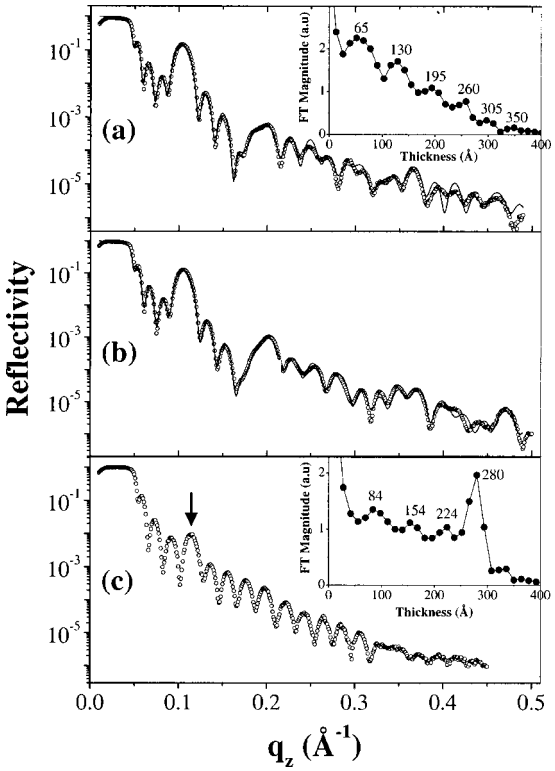

FIG. 11. XRR scans (open circles) and calculated reflectivities (line) of (a) as-deposited $(35\,\text{Nb}/35\text{Si})_5$ multilayer sample on float glass substrate and annealed at (b) 200 °C and (c) 300 °C. The vertical arrow in (c) indicates the position of the first order Bragg peak in the sample annealed at 300 °C. The inset in (a) and (c) show their corresponding Fourier transformations of the measured reflectivity data. The line connecting the closed circles is a guide to the eye.

order with three subsidiary oscillations between the Bragg peaks (characteristic of a five bilayer structure) arising due to total thickness of the film. The periodicity of the structure determined from the fit is 67.0 Å which is close to the nominal period of 70.0 Å. Since the thickness ratio of Nb and Si layers are 1:1, this gives rise to a reduction in reflectivity of the even order Bragg reflections.[38] The observed reduction in the intensity of all higher order Bragg reflections implies that the electron density modulation along the surface normal is close to sinusoidal.[39] Further, irregular interference oscillations observed at higher q_z values suggests that the deposited layer structure is deteriorated deeper into the stack.

For analysing the XRR data of a multilayer structure, we started with the EDP obtained from the trilayer films and extended it for the case of five bilayers. It was initially assumed that the EDP at all the Nb-on-Si interfaces are identical to that observed in the corresponding interface of the trilayer film. A similar assumption was made for all the Si-on-Nb interfaces. The reflectivity calculated in this manner resulted in considerable discrepancy with the measured data as the reflectivity of higher order Bragg reflections were considerably over estimated. For fitting the data, 50 boxes each of 6.85 Å size were considered. The average density ρ_0 and linear absorption coefficient μ for the average film were taken as 1.5 e/Å^3 and 6.7×10^{-6} Å^{-1}, respectively. Using these as the initial parameters, a nonlinear least square fitting using the box model resulted in a very good matching with

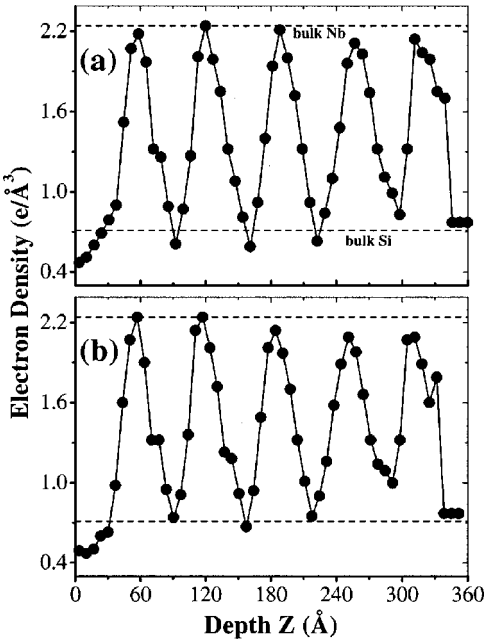

FIG. 12. EDPs (closed circles) of (a) as-deposited $(35\ \text{Nb}/35\ \text{Si})_5$ multilayer sample on float glass substrate and (b) annealed at 200 °C. The line connecting the closed circles is a guide to the eye.

the measured data. Substantial simulation study of the effect of variation in the electron densities of boxes at different depths was carried out before performing a fitting operation to get a set of parameters which are physically meaningful. The EDP of the as-deposited multilayer obtained from the fit is shown in Fig. 12(a). It is evident from the EDP that the electron density modulation is indeed close to sinusoidal. It can also be observed that interdiffusion is higher in the bottom layers of the stack. The widths of the first two interfaces from the top, i.e., Si-on-Nb and Nb-on-Si are 21 and 28 Å, respectively. In the last two interfaces, interdiffusion is higher with no clear demarcation between Si-on-Nb and Nb-on-Si. These observations lead one to conjecture that the bottom layers in the stack are annealed during deposition for considerably longer duration compared to the top layers. This is particularly true when the deposition is carried out with an extremely slow rate of the order of 0.1 Å/s. Under such deposition conditions, initial deposited layers are exposed to heat radiated from the evaporation source for longer time duration, causing more intermixing.

The ACF of the density gradient [Inset of Fig. 11(a)] for the as-deposited multilayer sample show peaks at 65, 130, 195, 260, 305, and 350 Å. The first four peaks correspond to the top four bilayer period positions in the stack. The individual layer thicknesses are not observed as the peaks are broadened due to the large interfacial width.[27] Moreover, splitting of the last bilayer period into two peaks at 305 and 350 Å is observed which reveals that there exists some qualitative difference in the EDP of the last bilayer compared to the other bilayers. This effect is also seen in the EDP shown in Fig. 12(a) where the last three layers show a different nature compared to the other layers.

The multilayer sample was annealed in the same manner as that of bilayer and trilayer samples. No noticeable change was observed in the XRR data of the sample annealed at 100 °C and hence is not shown here. Figure 11(b) shows the measured and fitted XRR spectra of the multilayer sample annealed at 200 °C. The observed shift in the Bragg reflections to higher q_z values correspond to a decrease in the bilayer period to 66 Å. This contraction of the bilayer period is attributed to the formation of a niobium silicide phase which is denser than the mixture of Nb and Si consumed in the reaction. This is a general trend observed in the case of metal/Si multilayers and has been reported by several groups.[6,13] For fitting the data, the box size was decreased from 6.85 to 6.7 Å and the number of boxes were kept the same to account for the contraction in the period. The corresponding EDP [Fig. 12(b)] shows considerable increase in interdiffusion at all the interfaces.

Measured XRR spectrum of the sample annealed at 300 °C [Fig. 11(c)] shows near total destruction of the multilayer structure. The first order Bragg reflection [marked by vertical arrow in Fig. 11(c)] is barely visible above the subsidiary oscillations which arise due to total thickness of the film. A very large shift in the first order Bragg reflection to higher q_z values is observed due to considerable contraction of the multilayer period and is attributed to the formation of niobium silicide. A corresponding increase in the critical wave vector q_c (which is proportional to the square root of electron density) is observed which implies that densification of the multilayer structure has taken place. The percentage increase in the electron density of the sample annealed at 300 °C relative to the as-deposited sample calculated from q_c is 19% and corresponds to an electron density of 1.8 e/Å^3. Moreover, partial remanence of the multilayer structure is observed due to trace visibility of the first order Bragg reflection. This implies that some layering persists even after annealing at 300 °C. An attempt to fit the measured data with a film of uniform electron density equal to that of Nb_3Si over the entire film thickness was, however, unsuccessful. To verify this, Fourier transformation of the measured reflectivity data [inset of Fig. 11(c)] was carried out which revealed very valuable information. It can be observed that there are three small peaks at the positions 84, 154, and 224 Å followed by a large peak at 280 Å. The large peak at 280 Å implies that maximum density gradient exists at a depth of 280 Å resulting from contraction of the multilayer structure due to the formation of Nb_3Si. The reduction in total film thickness to 280 Å after annealing at 300 °C from 350 Å in the as-deposited sample indicates a decrease of 20%. The three small peaks observed in ACF show that local density fluctuations exist around these positions. Based on XTEM studies, it has been reported in the case of Mo/Si multilayers annealed at high temperatures that drastic physical deformation of the multilayer structure takes place yielding severely warped silicide layers.[13] Since it would be difficult to extract physically meaningful EDP owing to the complexity of the structure as revealed by the Fourier transformation, no attempt was made to fit the data.

V. CONCLUSIONS

A systematic study of the variation in electron density profile as a function of depth has been carried out in as-

deposited and annealed Nb-on-Si and Si-on-Nb bilayers, Nb–Si–Nb and Si–Nb–Si trilayer structures. The structural parameters obtained from these studies are extended to determine layer-by-layer EDP variation in as-deposited and annealed Nb/Si multilayer structures. The EDP approach adopted in the present investigations clearly bring out the following important features missing so far in the studies conducted on similar multilayer systems.

(i) The asymmetry in the interfacial profile observed in Nb/Si system has been unambiguously attributed to the different growth morphology of deposited single layer films of Nb and Si on substrate.
(ii) Si is found to be the dominant diffusing species in the temperature range involved in the study.
(iii) Nb_3Si is found to be the first phase to nucleate at the interfaces of samples annealed at 300 °C.

ACKNOWLEDGMENTS

The authors sincerely thank Dr. B. A. Dasannacharya for his constant encouragement, support, and fruitful discussions throughout the course of this work. The authors are thankful to Dr. V. Ganesan and P. Saravanan for the AFM measurements. The authors are thankful to Satish Potdar for the help rendered in sample preparation. One of the authors (N.S.) would like to thank CSIR, India for the research fellowship.

[1] *Physics, Fabrication and Applications of Multilayered Structures*, edited by P. Dhez and C. Weisbuch (Plenum, New York, 1988).
[2] D. G. Stearns, D. P. Gaines, D. W. Sweeney, and E. M. Gullikson, J. Appl. Phys. **84**, 1003 (1994).
[3] A. Chaiken, R. P. Michel, and M. A. Wall, Phys. Rev. B **53**, 5518 (1996).
[4] S. P. Murarka, Silicides for *VLSI Application* (Academic, Orlando, FL, 1983).
[5] A. Kloidt, K. Nolting, U. Kleineberg, B. Schmiedeskamp, U. Heinzmann, P. Müller, and M. Kühne, Appl. Phys. Lett. **58**, 2601 (1991).
[6] J. B. Kortright, St. Joksch, and E. Ziegler, J. Appl. Phys. **69**, 168 (1991).
[7] E. E. Fullerton, J. Pearson, C. H. Sowers, S. D. Bader, X. Z. Wu, and S. K. Sinha, Phys. Rev. B **48**, 17 432 (1993).
[8] W. H. Wang, H. Y. Bai, M. Zhang, J. H. Zhao, X. Y. Zhang, and W. K. Wang, Phys. Rev. B **59**, 10 811 (1999).
[9] M. Zhang, W. Yu, W. H. Wang, and W. K. Wang, J. Appl. Phys. **80**, 1422 (1996).
[10] M. Zhang, W. Yu, and W. K. Wang, J. Mater. Sci. Lett. **16**, 241 (1997).
[11] T. Nakanishi, M. Takeyama, A. Noya, and K. Sasaki, J. Appl. Phys. **77**, 948 (1995).
[12] J. Y. Cheng and L. J. Chen, J. Appl. Phys. **69**, 2161 (1991).
[13] D. G. Stearns, M. B. Stearns, Y. Cheng, J. H. Stith, and N. M. Ceglio, J. Appl. Phys. **67**, 2415 (1990).
[14] C. Thompson, G. Palasantzas, Y. P. Feng, S. K. Sinha, and J. Krim, Phys. Rev. B **49**, 4902 (1994).
[15] S. Banerjee, M. K. Sanyal, A. Datta, S. Kanakaraju, and S. Mohan, Phys. Rev. B **54**, 16 377 (1996).
[16] M. K. Sanyal, J. K. Basu, A. Datta, and S. Banerjee, Europhys. Lett. **36**, 265 (1996).
[17] M. Yamamoto and T. Namioka, Appl. Opt. **31**, 1622 (1992).
[18] S. M. Chaudhari, N. Suresh, D. M. Phase, A. Gupta, and B. A. Dasannacharya, J. Vac. Sci. Technol. A **17**, 242 (1999).
[19] G. S. Lodha, S. Pandita, A. Gupta, R. V. Nandedkar, and K. Yamashita, Appl. Phys. A: Mater. Sci. Process. **62**, 29 (1996).
[20] M. Pattabi, N. Suresh, S. M. Chaudhari, A. Banerjee, D. M. Phase, A. Gupta, and K. Mohan Rao, Thin Solid Films **322**, 340 (1998).
[21] S. K. Sinha, E. B. Sirota, S. Garoff, and H. B. Stanley, Phys. Rev. B **38**, 2297 (1988).
[22] L. G. Parratt, Phys. Rev. **95**, 359 (1954).
[23] L. Nevot and P. Croce, Rev. Phys. Appl. **15**, 761 (1980).
[24] S. K. Sinha, M. K. Sanyal, B. L. Carvalho, M. Rafailovich, J. Sokolov, X. Zhao, and W. Zhao, *Resonant Anomalous X-ray Scattering: Theory and Applications* (Elsevier Science B.V., New York, 1994).
[25] F. Bridou and B. Pardo, J. Phys. III **4**, 1523 (1994).
[26] W. H. Press, S. A. Teukolsky, W. T. Vellerling, and B. P. Flannery, *Numerical Recipes in FORTRAN*, 2nd ed. (Cambridge University Press, Cambridge 1992).
[27] A. de Bernabe, M. J. Capitan, H. E. Fischer, and C. Prieto, J. Appl. Phys. **84**, 1881 (1998).
[28] J. P. Schlomka, M. Tolan, L. Schwalowsky, O. H. Seeck, J. Stettner, and W. Press, Phys. Rev. B **51**, 2311 (1995).
[29] A. K. Petford-Long, M. B. Stearns, C. H. Chang, S. R. Nutt, D. G. Stearns, N. M. Ceglio, and A. M. Hawryluk, J. Appl. Phys. **61**, 1422 (1987).
[30] K. Holloway, K. B. Do, and R. Sinclair, J. Appl. Phys. **65**, 474 (1989).
[31] M. Veldkamp, H. Zabel, and Ch. Morawe, J. Appl. Phys. **83**, 155 (1998).
[32] Ch. Morawe and H. Zabel, J. Appl. Phys. **77**, 1969 (1995).
[33] D. G. Stearns, J. Appl. Phys. **65**, 491 (1989).
[34] JCPDS Files, International Center for Diffraction data, Swarthmore, PA (1988).
[35] B. D. Cullity, *Elements of X-ray Diffraction* (Addison-Wesley, Reading, MA, 1978), p. 103.
[36] F. R. Boer, R. Room, A. R. Miedeme, and A. K. Niessen, *Cohesion in Metals* (North-Holland, Amsterdam, 1988).
[37] R. Pretorius, Vacuum **41**, 1038 (1990).
[38] J. H. Underwod and T. W. Barbee, Appl. Opt. **20**, 3027 (1981).
[39] H. L. Bai, E. Y. Jiang, C. D. Wang, and R. Y. Tian, J. Phys.: Condens. Matter **8**, 8763 (1996).